ACS Sustainable Chemistry & Engineering

Research Article

pubs.acs.org/journal/ascecg

Cellulose Nanoparticles: Structure–Morphology–Rheology Relationships

Mei-Chun Li,[†] Qinglin Wu,*[,†] Kunlin Song,[†] Sunyoung Lee,[‡] Yan Qing,[§] and Yiqiang Wu*[,§]

[†]School of Renewable Natural Resources, Louisiana State University AgCenter, Baton Rouge, Louisiana 70803, United States

[‡]Department of Forest Products, Korea Forest Research Institute, Seoul 130-712, Korea

[§]College of Materials Science and Engineering, Central South University of Forestry and Technology, Changsha 410004, China

ABSTRACT: The present study aims to investigate the structure–morphology–rheology relationships for cellulose nanoparticles (CNPs), including cellulose nanofibers (CNFs) and cellulose nanocrystals (CNCs). CNCs were extracted from never dried CNFs using sulfuric acid with controlled hydrolysis time. The crystalline structure, surface charge, morphology, and rheological behavior of the CNPs were measured and contrasted. The CNF suspensions exhibited rigid solid-like viscoelastic behavior even at a low concentration due to the formation of a highly entangled network. Upon acid hydrolysis, the network of rigid, long, and highly entangled nanofibers was eliminated, resulting in a significant loss of viscoelastic properties. Both steady-state and dynamic rheological measurements showed that the rheological behavior of the CNC suspensions was strongly dependent on the concentration and acid hydrolysis time. The CNC suspensions exhibited elastic gel-like rheological behavior at high concentrations but viscous liquid-like rheological behavior at low concentrations. Longer acid hydrolysis time produced CNCs with a lower aspect ratio, leading to higher critical transition concentration for the formation of anisotropic phase. The aspect ratio of CNCs was predicted from the intrinsic viscosity using the Simha's equation. The theoretically predicted aspect ratio values corresponded well with the transmission electron microscopy results. Finally, the network of CNF and CNC suspensions were schematically proposed.

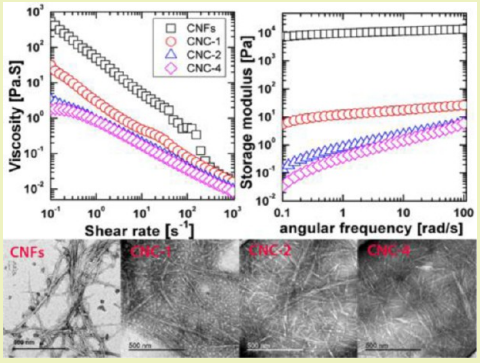

KEYWORDS: *Cellulose nanofibers, Cellulose nanocrystals, Structure, Rheological properties, Aspect ratio*

INTRODUCTION

Cellulose is the most abundant natural resource on earth with wide presence in wood, plants (e.g., cotton, jute, flax, hemp, sisal, coir, ramie, abaca, and kenaf), marine animals (e.g., tunicates), algae (e.g., red, green, gray, and yellow-green), and bacteria. Cellulose nanoparticles (CNPs), including cellulose nanofibers (CNFs) and cellulose nanocrystals (CNCs), can be extracted from cellulose through acid hydrolysis, enzyme treatment, mechanical disintegration, and 2,2,6,6-tetramethyl-1-piperidinyloxy (TEMPO)-mediated oxidation. Because of the large surface area, high aspect ratio, high Young's modulus, low cost, light weight, abundance, renewability and biodegradability, CNPs have been applied as multifunctional agents in various fields, for example, engineering composites,[1] paper,[2] package films,[3,4] biomedical materials,[5] hydrogels,[6] aerogels,[7] magnetic nanorods,[8] and supercapacitors.[9]

The performances of CNP-based materials are strongly dependent on their characteristics, such as three-dimensional size, aspect ratio, crystallinity, surface charge, dispersion microstructure, and rheological properties. Among the CNPs, CNFs exhibited stronger reinforcement than CNCs in a polymer matrix because CNFs had a much larger aspect ratio and stronger percolation network.[1] The optical performances of self-assembled CNC films were dependent on the dispersion microstructure of CNCs in an aqueous solution.[10] By tuning the cholesteric pitch structure of CNC suspensions, desired optical properties of cast CNC films were achieved. It seems that through tailoring the characteristics of CNPs final products with desirable properties can be achieved. Therefore, investigations on the processing, structure, morphology, and rheological behavior of CNPs are of considerable scientific interest and of great practical significance. Understanding these relationships can help us fully exploit the capabilities of CNPs.

Rheological measurements have been applied to characterize the CNF and CNC suspensions over the past few years. It has been known that CNFs exhibited pseudoplastic and thixotropic behaviors.[11−15] The increase in the number of homogenization treatments enhanced the delamination of nanofibers, leading to an increase in the viscosity and elastic modulus of CNF suspensions.[11,12] On the contrary, an increase in the TEMPO oxidation time decreased the elastic modulus of CNF suspensions, which was caused by the reduction in the length as well as the entangled network of nanofibers.[13] Moreover, freeze-drying treatment also led to loss of elastic modulus of CNFs, which might be caused by the formation of nanofiber bundles during lyophilization.[15] CNFs fabricated from different

Received: December 8, 2014
Revised: March 22, 2015
Published: March 30, 2015

DOI: 10.1021/acssuschemeng.5b00144
ACS Sustainable Chem. Eng. 2015, 3, 821−832

cellulose materials showed distinctive rheological properties, owing to differences in chemical composition, crystallinity, length, aspect ratio, and manufacturing steps.

The rheological behavior of CNC suspensions is also of great interest because most of the CNC-based materials are fabricated from the CNC and/or CNC/polymer suspensions using a casting method. Besides, the rheological behavior helps reveal the dispersion microstructure of the CNC suspension, which can be divided into four types: isotropic structure, biphasic sturcture of isotropic and liquid crystalline, liquid crystalline structure, and gel-like structure.[16−23] Previous investigations showed that the rheological behavior of CNC suspensions as well as the critical concentrations for the phase transition from one dispersion microstructure to another were dependent on the characteristics of CNCs (e.g., aspect ratio and surface charge), pretreatment (e.g., applied ultrasound energy), and post-treatment (e.g., addition of electrolytes). Shafiei-Sabet el al.[17−19] investigated the influence of ultrasound energy, surface charges, and ionic strength on the rheological properties of CNC suspensions. They found that the critical transition concentrations were shifted to higher values when more ultrasound energy was applied or when the CNCs had higher surface charges or when more NaCl was added. Dong et al.[21] indicated that the phase separation was mainly governed by particle geometry and ionic strength, and the addition of electrolytes also increased the critical concentration.

Although studies have been done to investigate control parameters for the rheological behavior of CNP suspensions, systematic data on the structure−morphology−rheology relationships are very limited. Furthermore, to our knowledge, most of the previous studies solely dealt with the rheological behavior of individual CNF or CNC suspensions. To date, there is no comprehensive comparative investigation on the rheological properties between CNF and CNC suspensions from the same cellulose material. In the present study, CNCs with different aspect ratios were extracted from CNFs using acid hydrolysis with controlled hydrolysis time. The crystallinity, surface charge, morphology, and rheological properties between CNFs and CNCs were directly compared. The objectives of the study were (1) to evaluate the influence of hydrolysis time on the characteristics of obtained CNPs, (2) to comprehensively compare the rheological behavior of the CNF and CNC suspensions, and (3) to establish the relationships between the aspect ratio of CNCs and their suspensions' rheological behavior using both rheological measurement and theoretical modeling. It is expected that more detailed understanding of these relationships provides us more fundamental guidance for the development of sustainable CNP-based materials with finely controlled properties.

EXPERIMENTAL SECTION

Materials and Sample Prepration. *Materials.* Microfibrillated cellulose (Celish KY 100-S grade, 25% solid content) in the form of CNFs was purchased from Daicel Chemical Industries, Ltd. (Tokyo, Japan). Microfibrillated cellulose was fabricated from highly refined pure plant fiber materials through strong mechanical shearing forces in a superhigh-pressure homogenizer. Sulfuric acid (95−98 wt %, reagent grade) was purchased from Sigma-Aldrich Corp. (St. Louis, MO, U.S.A.), which was diluted to 64 wt % before use. All water used was deionized water.

Preparation of CNF Suspensions. Never dried CNF samples were added into deionized water with vigorous mechanical stirring at a speed of 2000 rpm for 1 h. The resultant CNF suspensions were then diluted into 1.5, 1.0, 0.5, and 0.25 wt % using deionized water for the rheological measurements.

Preparation of CNC Suspensions. CNCs were extracted from CNFs using the acid hydrolysis method.[24] Never dried CNFs were added into 64 wt % sulfuric acid, followed by mechanically stirring at 45 °C for 1, 2, and 4 h. After reaction, the slurries were poured into a 2000 mL plastic container with excess deionized water to terminate the reaction. At rest, the suspensions precipitated quickly. The supernatant was removed, and the sediment was collected carefully. Then, the collected sediment was redispersed in fresh deionized water. The process of redispersion and separation was repeated several times until the pH reached to 3−4. Finally, the suspensions were poured into regenerated cellulose dialysis tubes. The tubes were placed in a large water tank to dialyze against the deionized water for several days until the pH reached around 6−8. The sulfuric acid-hydrolyzed CNCs from the CNFs with acid hydrolysis times of 1, 2, and 4 h were designated as CNC-1, CNC-2, and CNC-4, respectively. In order to further decrease the particle size of the CNCs, a high-pressure homogenizer (Microfluidizer M-110P, Microfluidics Corp., Newton, MA, U.S.A.) was used to treat the CNC suspensions.[25] The CNC suspensions were pumped to go through a pair of Z-shaped interaction chambers (one 200 μm ceramic and one 87 μm diamond) five times at an operating pressure of 207 MPa. The resultant CNC suspensions were stored in a sealed glass container and placed in a refrigerator at 5 °C to avoid water evaporation. Finally, the CNC suspensions were adjusted to 1.5, 1.0, 0.5, and 0.25 wt % by slowly evaporating the water or adding the deionized water for the rheological measurements.

Freeze-Drying of CNFs and CNCs. A certain amount of 1 wt % of CNF or CNC suspensions was poured into a fast-freeze-drying flask. The suspensions were frozen quickly at −75 °C for about 2 h in a freezer. Then, the completely frozen samples were immediately shifted to a freeze-dryer (FreeZone plus 2.5 L, Labconco Corp., Kansas, MO, U.S.A.) at a sublimating temperature of −50 °C for 5 days.

Crystalline and Surface Structure Characterization. *Wide-Angle X-ray Diffraction (WXRD).* WXRD patterns of freeze-dried CNF and CNC samples were measured using a Bruker Siemens D5000 X-ray diffractometer operated at the Cu Kα radiation (λ = 0.154 nm) with 40 kV and 30 mA in a 2θ range from 5° to 40° at a step size of 0.02°. The crystalline index (CI) of each sample was calculated according to Segal et al.[26] using the following equation:

$$\mathrm{CI}\,(\%) = \frac{I_{200} - I_{\mathrm{Am}}}{I_{200}} \times 100\% \quad (1)$$

where I_{200} is the maximum intensity of the (200) lattice diffraction peak, and I_{Am} is the intensity scattered by the amorphous fraction of the sample.

Zeta Potential. The zeta potential values of 0.05 wt % CNF and CNC suspensions were determined using a ZetaTrac analyzer (MicroTrac Inc., Largo, FL, U.S.A.). Reported values are an average of 10 measurements.

X-ray Photoelectron Spectroscopy (XPS). XPS spectra of freeze-dried CNF and CNC samples were collected using a Specs PHOIBOS-100 spectrometer (SPECS, Berlin, Germany) with a Al Kα irradiation (1486.61 eV) at 10 kV and 10 mA current. Survey spectra were recorded from 1200 to 0 eV at a pass energy of 40 eV with a scan step of 1.0 eV. High-resolution S 2p spectra were recorded at pass energy of 40 eV with a scan step of 0.1 eV. High-resolution S 2p spectra were smoothed using the Origin 8.0 software. The mass concentrations were determined using the SpecLab software. With the reported molecular formula for acid-treated CNCs of $C_6H_{10}O_5$-$(SO_3)_n$,[27] the number (n) of sulfate groups per 100 bulk anhydroglucose units was calculated based on the following equation

$$n = \frac{100 \times 162.14 \times S}{32.065 - 80.065 \times S} \quad (2)$$

where S (wt %) is the mass concentration of sulfur element in acid-treated CNC samples.

Morphology Characterization. *Transmission Electron Microscopy (TEM).* Never dried CNF and CNC suspensions were diluted to

DOI: 10.1021/acssuschemeng.5b00144
ACS Sustainable Chem. Eng. 2015, 3, 821−832

0.1 wt % using deionized water, followed by ultrasonic treatment for 1 h. Specially, the resultant CNF suspensions were further treated in the high-pressure-homogenizer 10 times in order to improve the dispersion state of CNFs. A droplet (5 μL) of diluted CNF or CNC suspensions was deposited in a 300-mesh Lacey Carbon Film (LC300-CU-100) and then negatively stained with 2 wt % uranyl acetate solution for about 2 min to enhance the sample contrast. All samples were analyzed using a transmission electron microscope (JEM 1400, JEOL) with an accelerating voltage of 120 kV. The average length and width of the particles was calculated based on 50 randomly chosen nanofibers from the TEM images using ImageJ 1.47 software (http://rsb.info.nih.gov.libezp.lib.lsu.edu/ij/).

Field Emission-Scanning Electron Microscopy (FE-SEM). Microstructure and surface morphology of freeze-dried CNF and CNC foam samples were observed using a field emission scanning electron microscopy (FE-SEM, a FEI QuantaTM 3D FEG dual beam SEM/FIB system, Hillsboro, Oregon, U.S.A.) at a 20 kV accelerating voltage. Before observations, all samples were deposited on carbon tape mounted on an aluminum stub and sputter coated with gold for 2 min. The average width of particles was calculated based on 50 randomly chosen particles from the FE-SEM images using ImageJ 1.47 software.

Rheological Measurements. Rheological properties of CNF and CNC suspensions were measured using a stress-controlled rheometer (AR 2000, TA Instrument, Inc., New Castle, DE, U.S.A.) with a cone-and-plate geometry (cone angle, 2°; diameter, 40 mm; truncation, 56 μm) at 25 °C. Steady-state viscosity was performed in a shear rate range from 0.01 to 1000 s^{-1}. Strain sweep was conducted to determine the linear viscoelastic region before each frequency sweep. Strain sweep measurements were performed within a strain range from 0.01% to 100% at a fixed frequency of 1 Hz. Frequency sweep measurements were carried out over an angular frequency range from 0.1 to 100 rad/s within the linear viscoelastic region.

RESULTS AND DISCUSSION

Crystalline and Surface Structures of CNFs and CNCs. WXRD patterns of freeze-dried CNFs and CNCs are shown in Figure 1. All samples exhibited four major diffraction peaks at around 15.2°, 16.7°, 22.6°, and 34.5°, corresponding to the cellulose I crystallographic planes 1$\bar{1}$0, 110, 200, and 004, respectively.[28,29] Acid hydrolysis and an increase in hydrolysis time did not cause any change in the diffraction peak position of CNFs, revealing that acid hydrolysis did not alter the crystalline structure of CNFs. However, the crystallinity index (CI) was slightly changed as the hydrolysis time increased. The CI values calculated from Figure 1 using eq 1 for CNFs, CNC-1, CNC-2, and CNC-4 were 70.5%, 71.7%, 72.2%, and 74.2%, respectively. The small CI change from 70.5% (CNFs) to 71.7% (CNC-1) indicated that the 1 h acid hydrolysis time was not enough to eliminate all amorphous regions in CNFs. The CNFs used were prepared through mechanical disintegration method. Although the pretreatments removed the majority of noncellulosic materials (e.g., hemicellulose and lignin) from raw fibers, a small amount of noncellulosic materials might still exist in CNFs,[15,30,31] which covered the surface of CNFs, resulting in the reduction in hydrolysis efficiency. Nevertheless, the continuous increase in the CI values from 70.7% to 74.2% demonstrated that the amorphous region in CNFs was gradually digested in 64 wt % sulfuric acid solution, leading to the production of CNCs with smaller dimensions.

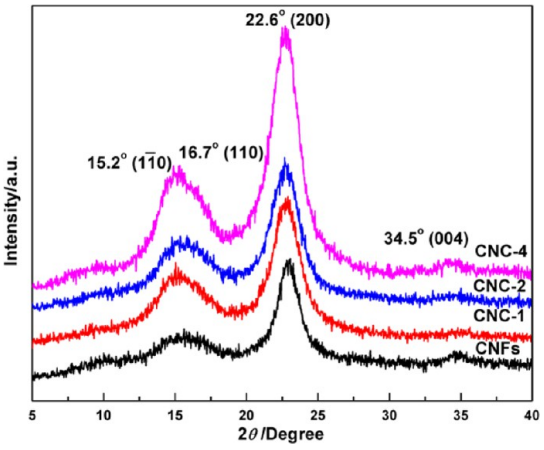

Figure 1. XRD patterns of CNFs and CNCs.

Sulfuric acid-hydrolyzed CNCs contained negative electrical charges due to the introduction of sulfate groups ($-O-SO_3^-$) on their surface. The amount of sulfate groups can be tailored by the change in the sulfuric acid concentration and the hydrolysis time. Generally, high sulfuric acid concentration and longer hydrolysis time generate CNCs with more sulfate groups on the surface. Table 1 presents the zeta potential values of the CNFs and CNCs. The CNFs had a negative zeta potential value of -4.6 ± 1.2 mV, probably due to the existence of carboxylic acid groups on the surface.[32,33] It is well known that in order to remove lignin from the raw fibers, $NaClO_2$/acetic acid were usually added.[34] The addition of $NaClO_2$ during delignification might partially oxidize the cellulose, producing a few of carboxylic acid groups on the surface of CNFs. The carboxylic acid has a pK_a value lower than 7, and thus, at the neutral CNF suspensions, the deprotonation of carboxylic acid occurred, giving negatively charged carboxylate anions. Upon acid hydrolysis for 1, 2, and 4 h, the zeta potential values were decreased to -12.8 ± 1.8, -26.3 ± 2.5, and -35.4 ± 2.0 mV, respectively, revealing that more and more sulfate groups attached to the surface of CNCs. The zeta potential also reflected the stability of colloidal suspensions. In general, a colloidal suspension with high zeta potential larger than $\pm$30 mV has good stability, with moderate zeta potential ranging from $\pm$10 to $\pm$30 mV has incipient instability, and with low zeta potential ranging from 0 to $\pm$5 mV will rapidly flocculate.[35] Therefore, as shown in Figure 2, CNFs flocculated rapidly to the bottom of vial within 1 h, while CNCs were well dispersed in the aqueous solution for 3 months. Moreover, it was observed that as the hydrolysis time increased, the color of CNP suspension gradually changed from white to white purple

Table 1. Physicochemical Characteristics of CNFs and CNCs

		atomic concentration (atom %)			mass concentration (wt %)				
sample	zeta potential (mV)	C	O	S	C	O	S	OSO_3H/100 anhydroglucose units	aspect ratio
CNFs	-4.6 ± 1.2	56.07	43.93	0	48.93	51.07	0	0	>80
CNC-1	-12.8 ± 1.8	56.34	43.58	0.08	49.15	50.67	0.18	0.91	55.1 ± 20.4
CNC-2	-26.3 ± 2.5	51.91	47.90	0.19	44.66	54.90	0.44	2.25	48.9 ± 17.5
CNC-4	-35.4 ± 2.0	54.62	45.15	0.23	47.34	52.13	0.53	2.72	37.8 ± 15.2

DOI: 10.1021/acssuschemeng.5b00144
ACS Sustainable Chem. Eng. 2015, 3, 821−832

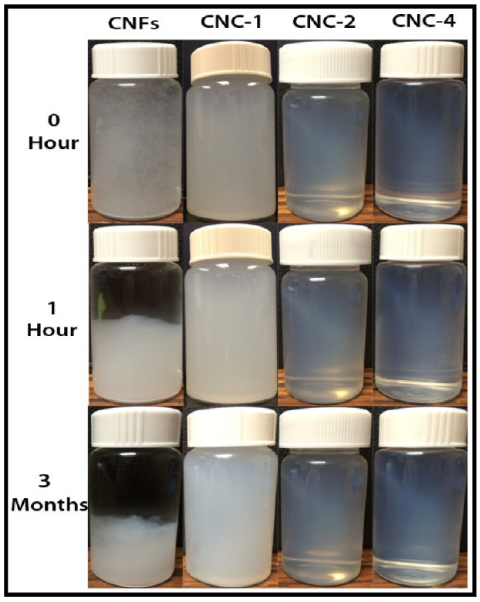

Figure 2. Dispersion state of CNF and CNC suspensions at the concentration of 1 wt % with different standing times.

to transparent light purple due to the reduction in the three-dimensions of the CNPs.

In order to quantitatively evaluate the number of sulfate groups, the chemical compositions of CNFs and CNCs were analyzed using XPS. Figure 3a shows the XPS survey spectra peaks of CNFs and CNCs. The peaks at 1071.8, 530.5, 284.5, and 167.0 eV were observed for all samples, originating from Na 1s, O 1s, C 1s, and S 2p, respectively.[36] A small amount of Na atoms was detected, which might be impurities introduced during the alkali and bleaching treatments of the raw fibers. Hydrogen atoms were not detected by the XPS. The S 2p peak region in the survey spectra was further determined using high-resolution analysis, as shown in Figure 3b. It is evident that the S 2p peak was absent in the spectrum of CNFs. However, in the spectra of CNCs, the S 2p peak was observed. The intensity of the S 2p peak gradually increased with an increase in acid hydrolysis time, indicating that more sulfate groups were introduced on the surface of CNCs. The mass concentrations of C, O, and S elements are summarized and listed in Table 1. The mass concentration of the S element was 0.18%, 0.44%, and 0.53%, corresponding to 0.91, 2.25, and 2.72 sulfate groups per 100 anhydroglucose units for CNC-1, CNC-2, and CNC-4, respectively.

Morphology of CNFs, CNCs, and Their Freeze-Dried Materials. Figure 4a shows the TEM micrograph of CNFs. As shown in Figure 4a, a few individual nanofibers with widths of 12.52 ± 8.43 nm and lengths up to several micrometers were observed. Most nanofibers appeared as bundles or clusters with widths of 20−50 nm. It was difficult to accurately calculate the lengths of the nanofibers because they were strongly aggregated or twisted, even though the homogenization was applied. The created highly entanged network had a significant influence on the viscoelastic rheological properties of CNF suspensions (to be discussed in the rheological part). Figure 4d, g, and j show the TEM micrographs of CNC-1, CNC-2, and CNC-4, respectively. The CNCs exhibited a needle-like shape. Particularly, CNC-1 was 471.25 ± 150.12 nm in length and 8.56 ± 6.44 nm in width. Thus, upon acid hydrolysis for 1 h, both the lengths and widths of the CNFs were reduced, indicating that acid not only longitudinally cut the nanofibers but also crosswise defibrillated the nanofibers. In comparison with the width change, the reduction in length was more evident. It was also evident that some long nanofibers still existed after 1 h of sulfuric acid hydrolysis. With an increase in hydrolysis time from 1 to 4 h, both the widths and lengths of the CNCs further decreased. The average length and width of the CNCs were 346.51 ± 90.64/7.08 ± 5.21 and 228.36 ± 63.78/6.05 ± 3.53 nm for CNC-2 and CNC-4, respectively. Interestingly, it was observed that the polydispersity in length and width also consistently decreased with an increase in hydrolysis time, suggesting that a more uniform dimension was achieved by increasing the hydrolysis time. The aspect ratio (length/width) of the CNCs played an important role in improving the chemical and physical performances of the CNC-based materials. Thus, the aspect ratio values of the CNFs and CNCs were calculated, as summarized in Table 1. The CNFs had a very high aspect ratio value (>80), and CNC-1, CNC-2, and CNC-4 had relatively lower aspect values of 55.05 ± 20.37, 48.94 ± 17.52, and 37.75 ± 15.17, respectively, showing a well decreasing trend with an increase in hydrolysis time from 1 to 4 h. The resultant CNCs had higher aspect ratio values than those of CNCs from other cellulosic materials, for example, microcrystalline cellulose,[24] cotton,[37] and kenaf fibers.[38]

FE-SEM micrographs of freeze-dried CNFs are presented in Figure 4b and c. After freeze-drying, the rigid entangled network of nanofibers was well kept. The majority of nanofibers

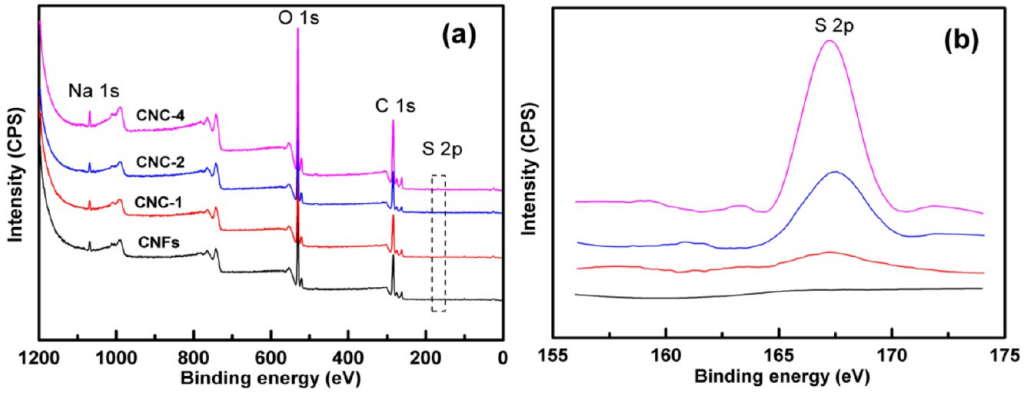

Figure 3. XPS survey spectra (a) and high-resolution of S 2p photoelectron spectra (b) of CNFs and CNCs.

DOI: 10.1021/acssuschemeng.5b00144
ACS Sustainable Chem. Eng. 2015, 3, 821−832

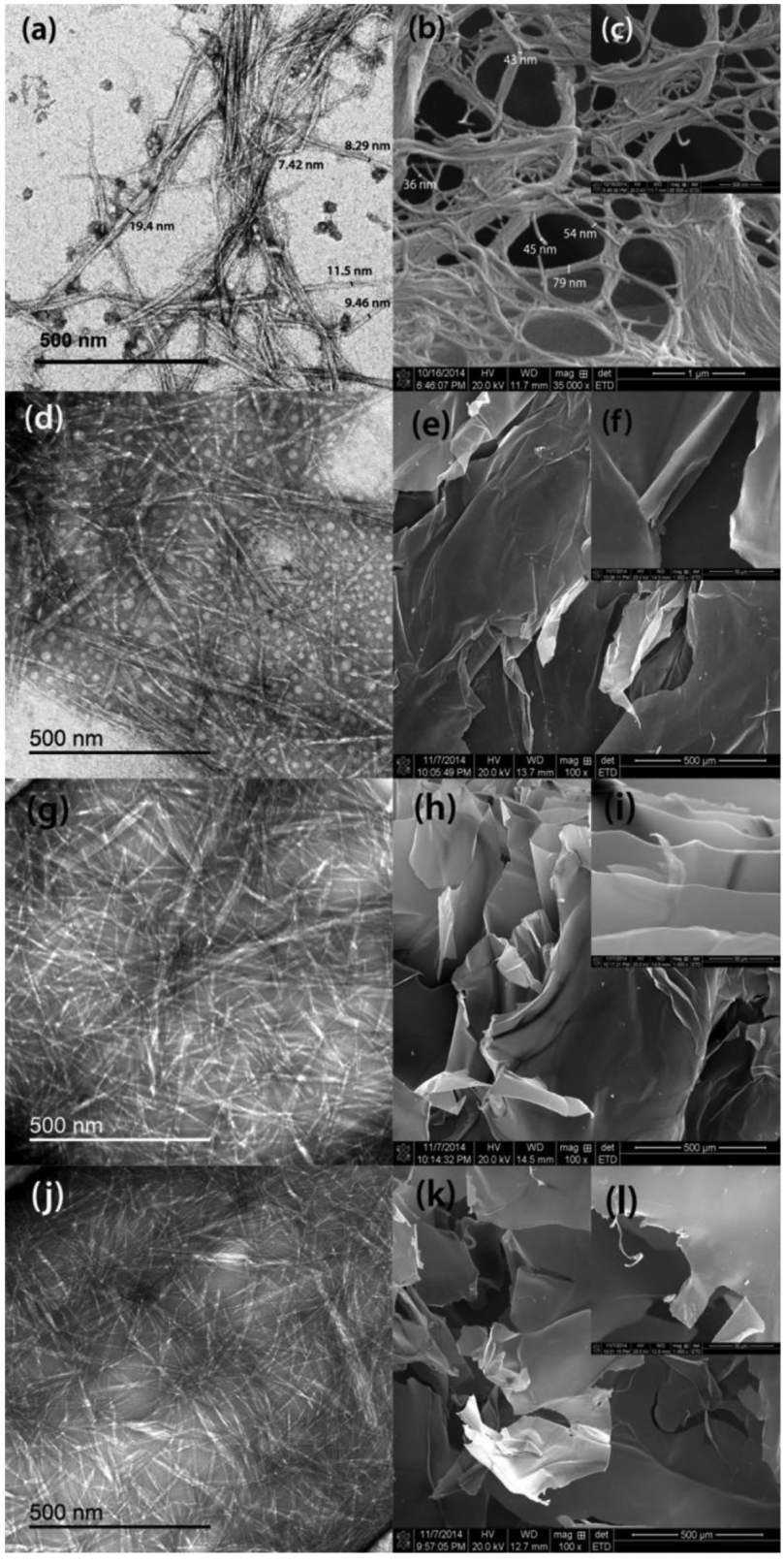

Figure 4. Morphology of CNFs, CNCs, and their freeze-dried materials. (a,d,g,j): TEM micrographs of CNFs, CNC-1, CNC-2, and CNC-4, respectively. (b,c), (e,f), (h,i), (k,l): FE-SEM micrographs of freeze-dried CNFs, CNC-1, CNC-2, and CNC-4, respectively. Scale bar: (a,c,d,g,j) = 500 nm; (b) = 1 μm; (e,h,k) = 500 μm; (f,i,l) = 50 μm.

appeared as bundles with widths of 30−100 nm. During the freeze-drying process, various individual nanofibers and smaller bundles were further aggregated. Therefore, the nanofiber bundles obtained after freeze-drying showed much larger widths in comparison with the nanofiber bundles without freeze-drying (Figure 4a). Figure 4e, h, and k show the FE-SEM micrographs of freeze-dried CNC-1, CNC-2, and CNC-4, respectively. Very different from the morphology of freeze-

DOI: 10.1021/acssuschemeng.5b00144
ACS Sustainable Chem. Eng. 2015, 3, 821−832

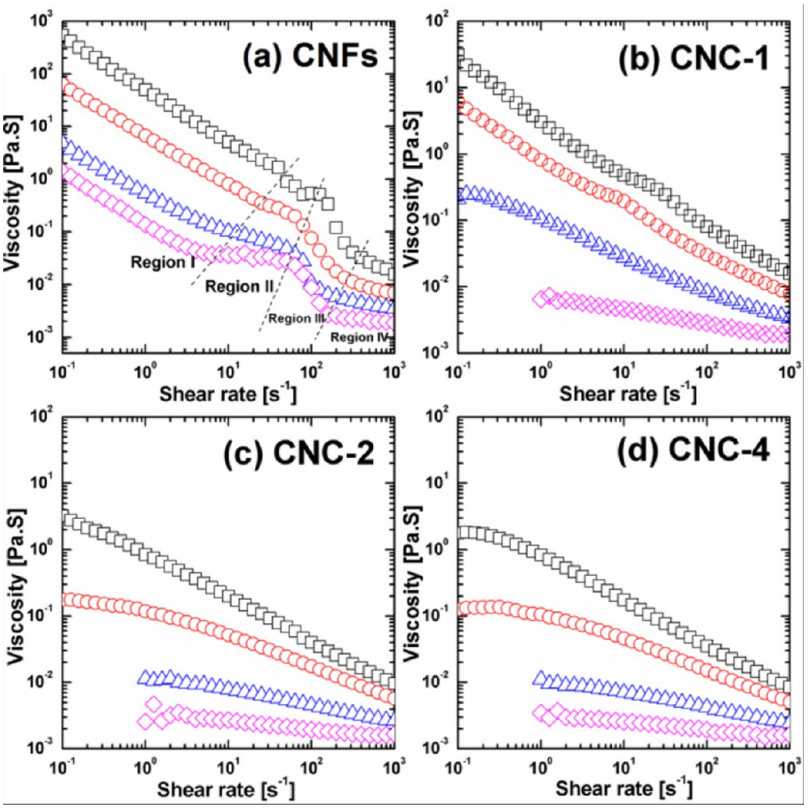

Figure 5. Steady-state viscosity versus shear rate of (a) CNFs, (b) CNC-1, (c) CNC-2, and (d) CNC-4 suspensions with concentrations of 1.5 wt % (black squares), 1.0 wt % (red circles), 0.5 wt % (blue triangles), and 0.25 wt % (magenta diamonds) at 25 °C. At a low concentration and low shear rate region, the viscosity could not be measured precisely because of the sensitivity of rheometer.

dried CNFs, the freeze-dried CNCs displayed a unique lamellar structure consisting of a large number of thin plates with thicknesess of about 1−2 μm. There was no individual CNCs, CNC bundles, or microsized fibers observed within each thin plate, as shown in Figure 4f, i, and l at high magnification. This observation suggested that during the freeze-drying process CNCs were self-assembled into thin membrane layers. In comparison to CNC-1, CNC-2 and CNC-4 displayed more significant lamellar structure, presumably owing to the more homogeneous dimension as well as the introduction of more sulfate groups on the surface of CNC-2 and CNC-4, which provided stronger electrostatic repulsion to fabricate self-assembled foam with more numbers of layers. Self-assembling behavior of CNPs during freeze-drying was reported previousely.[25,39,40] Han et al.[25] observed that the morphology of the self-assembled cellulose foam was dependent on the aspect ratio, concentration, hydrogen bonding, crystallinity, and surface charge of CNCs. They interpreted the mechanism of self-assembling behavior of cellulose nanoparticles during freeze-drying based on the orientation of ice crystals during growth, existence of hydrogen bonding between adjacent cellulose particles, and formation of ordered chiral nematic structure above the critical transition concentration. The present study demonstrated that CNCs with larger aspect ratios were also able to self-assemble into lamellar structure, revealing that the aspect ratio of CNCs had a slight influence on the self-assembling behavior of CNPs during freeze-drying. Furthermore, it was observed that CNFs were not able to self-assemble into layered membranes, as shown in Figure 4b and c. One reason is that the surface characteristic of the nanofiber was inactive with fewer hydroxyl groups. The other reason was due to the formation of a strongly entangled network, which largely prohibited the self-assembling of microsized fibers as well as the orientation of nanofibers in parallel to the movement of the freezing front.

Steady-Flow Rheological Behaviors of CNF and CNC Suspensions. Steady-state viscosities as a function of the shear rate of CNF suspensions with concentrations of 1.5, 1, 0.5, and 0.25 wt % are shown in Figure 5a. It was observed that higher concentrations resulted in increased viscosity along the whole shear-thinning curve, indicating that a more rigid network was created with an increase in the concentration of CNFs. Furthermore, the viscosity declined as the shear rate increased, displaying typical shear-thinning behavior. Interestingly, each shear-thinning curve can be divided into four characteristic regions. In regions I, the nanofibers slowly oriented along the shear direction under the low shear force, causing a gradual decrease of viscosity. In region II, the viscosity stopped decreasing and an evident plateau was observed. This behavior was more pronounced at a low concentration, such as 0.25 wt %. It was proposed that more entangled network was formed in this area, which prohibited the continuous reduction of viscosity.[41] Indeed, TEM observation (Figure 4a) showed that the nanofibers were very long, and thus, there was a strong possibility for nanofibers to create a more entangled network during shearing. In region III, as the shear rate continually increased, the high shear force caused the breakdown of the entangled network into individual nanofibers, leading to a sharp drop in the viscosity. In region IV, another plateau appeared because most of entangled network was disrupted and a well-oriented structure was formed. Different shear-thinning behaviors of CNF suspensions were reported in previous

DOI: 10.1021/acssuschemeng.5b00144
ACS Sustainable Chem. Eng. 2015, 3, 821−832

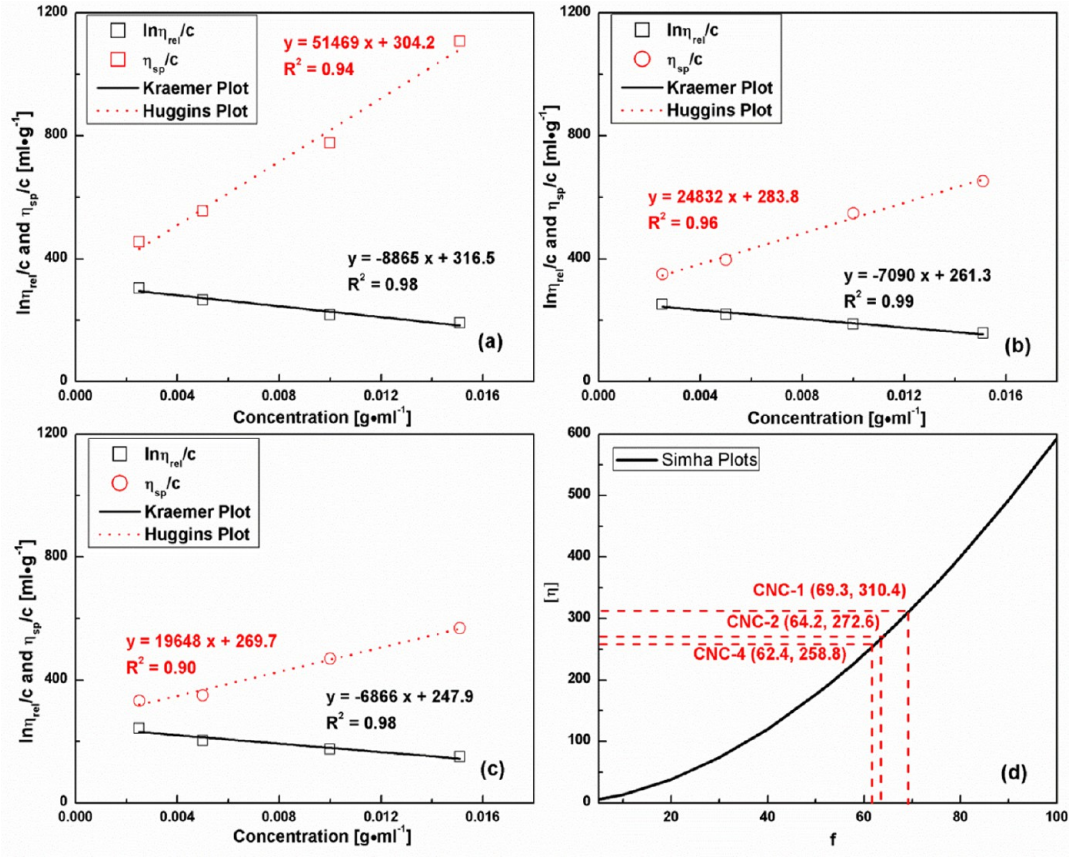

Figure 6. Values of ln η_{rel}/c and η_{sp}/c and plots of Kraemer and Huggins for CNC suspensions: (a) CNC-1, (b) CNC-2, and (c) CNC-4 at a shear rate of 1000 s^{-1} at 25 °C, and (d) Simha plot used to estimate the aspect ratio (f) of CNCs.

literatures. For example, Iotti et al.[41] found the three-region shear-thinning behavior of CNF suspensions derived from *Picae abies* pulp, whereas Rezayati Charani et al.[11] reported the linear shear-thinning behavior of CNF suspensions derived from kraft pulp. The present CNF suspensions exhibited closer shear-thinning behavior to that of CNF suspensions derived from *Picae abies* pulp than that of CNF suspensions derived from kraft pulp, presumably due to the difference in the aspect ratio. The nanofibers with the larger aspect ratio could produce a more shear-induced entangled network, exhibiting a more evident plateau region in the shearing curve.

Steady-state viscosities as a function of the shear rate of CNC-1, CNC-2, and CNC-4 suspensions with concentrations of 1.5, 1, 0.5, and 0.25 wt % are shown in Figure 5b, c, and d, respectively. For all CNC suspensions, the viscosity gradually increased as the concentration increased due to the growth in the collision possibility of CNCs. However, the viscosity monotonically declined as the shear rate increased over the whole investigated shear rate ranges, exhibiting a typical shear-shinning behavior. Furthermore, with an increase in acid hydrolysis time from 1 to 4 h (i.e., with a decrease in the CNC aspect ratio), the viscosity gradually declined. These results indicated that the viscosity of the CNC suspensions was strongly dependent on shear rate, CNC concentration, and CNC aspect ratio. It was reported that the CNC suspension displayed lyotropic phase behavior.[16−23] With increased CNC concentration, the CNC suspensions progressively transformed from an isotropic structure to a biphasic structure of isotropic and liquid crystalline, to a liquid crystalline structure, and finally to a gel-like structure. Distinctive shear-thinning behaviors were observed for the present CNC suspensions with different CNC concentrations and different CNC aspect ratios. For example, for the CNC-1 suspension at high concentrations (e.g., 1.5 and 1.0 wt %), a three-region shear-thinning behavior was observed, revealing the gel-like structure. The CNC-1 suspension with a moderate concentration (e.g., 0.5 wt %) exhibited a Newtonian plateau at low shear rates, followed by a shear-thinning region at high shear rates, corresponding to the biphasic structure of isotropic and liquid crystalline. At a low concentration (e.g., 0.25 wt %), the rheological behavior was nearly Newtonian, corresponding to its isotropic structure. For CNC-2 and CNC-4 suspensions, the Newtonian plateau occurred when the concentration was 1.0 and 1.5 wt %, respectively. Moreover, the three-region shear-thinning behavior was not found for the CNC-4 suspension at any concentration level. These observations revealed that the critical concentration for phase transition from anisotropic to isotropic was shifted to a higher value with a decrease in the CNC aspect ratio.

Steady-state rheological measurements showed that both CNF and CNC suspensions exhibited shear-thinning behaviors with some distinctive differences between them. First, at the same concentration level, CNF suspensions had a substantially higher viscosity than that of CNC suspensions. For example, at a shear rate of 1 s^{-1}, 1 wt % of CNF, CNC-1, CNC-2, and CNC-4 suspensions had viscosities of 6.714, 0.8158, 0.1188, and 0.1053 Pa s, respectively. Second, the CNF suspension behaved with a characteristic four-region shear-thinning behavior at any concentration level, while the shear-thinning behaviors of the CNC suspensions were strongly dependent on the concentration and aspect ratio of the CNCs. The CNC-1

DOI: 10.1021/acssuschemeng.5b00144
ACS Sustainable Chem. Eng. 2015, 3, 821−832

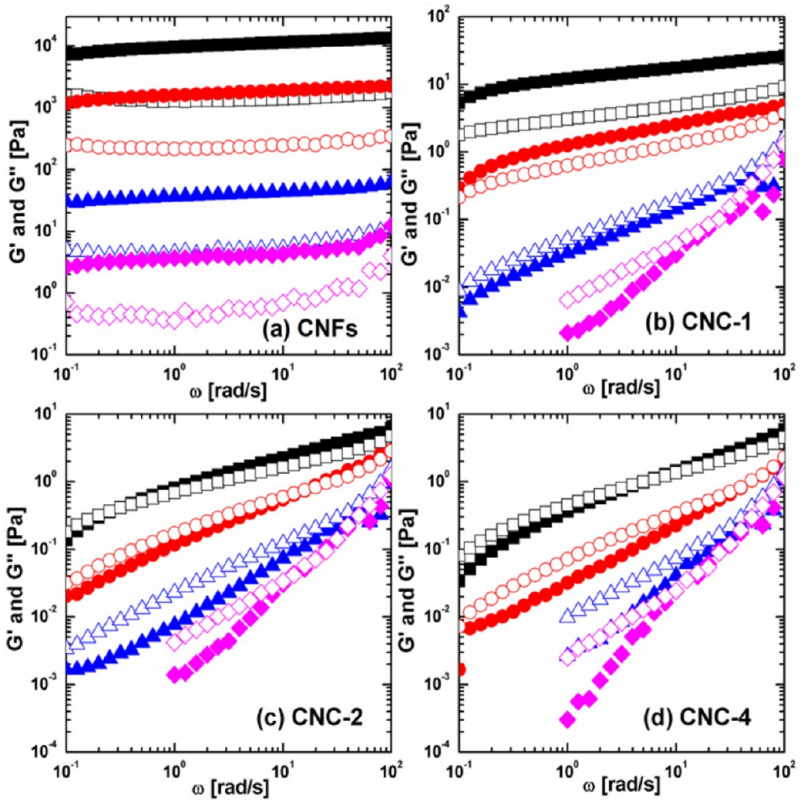

Figure 7. Storage modulus G' (solid symbols) and loss modulus G'' (open symbols) versus angular frequency ω of (a) CNFs, (b) CNC-1, (c) CNC-2, and (d) CNC-4 suspensions with concentrations of 1.5 wt % (black squares), 1.0 wt % (red circles), 0.5 wt % (blue triangles), and 0.25 wt % (magenta diamonds) at 25 °C.

suspensions at high concentrations (e.g., 1.5 and 1.0 wt %) exhibited three-region shear thinning behaviors, which was somewhat similar to the four-region shear-thinning behavior of the CNF suspension, presumably due to the existence of some long nanofibers in the CNC-1 suspensions (Figure 4d). As the aspect ratio of the CNCs decreased, the three-region shear-thinning behavior gradually disappeared. These findings provided us some useful information on identifying the type of CNPs or even predicting the aspect ratio of CNCs without using microscopic techniques (e.g., optical, electron, or scanning probe microscopy).

The aspect ratio (f) of rigid rod-like nanoparticles can be predicted from the intrinic viscosity $[\eta]$, according to the Simha equation[33,42−44]

$$[\eta] = \frac{f^2}{15(\ln 2f - 1.5)} + \frac{f^2}{5(\ln 2f - 0.5)} + \frac{14}{15} \tag{3}$$

The $[\eta]$, a measure of the contribution of individual particles to the total viscosity of a suspension,[45] can be determined by measuring the visocosity of the diluted CNC suspensions and using the Huggins and Kraemer's equations[46,47]

$$\frac{\eta_{sp}}{c} = [\eta] + k_1[\eta]^2 c \tag{4}$$

$$\frac{\ln \eta_{rel}}{c} = [\eta] + k_2[\eta]^2 c \tag{5}$$

where k_1, k_2, and c are the Huggins constant, Kraemer constant, and concentration of particles, respectively. η_{sp} and η_{rel} are the specific viscosity and relative viscosity, respectively, which are calculated as

$$\eta_{sp} = \frac{\eta - \eta_0}{\eta_0} \tag{6}$$

$$\eta_{rel} = \frac{\eta}{\eta_0} \tag{7}$$

where η is the viscosity of CNC suspensions, and η_0 is the visocosity of solvent (deionized water).

The $\ln \eta_{rel}/c$ and η_{sp}/c values for the CNC-1, CNC-2, and CNC-4 suspensions as a function of concentration at a shear rate of 1000 s^{-1} are shown in Figure 6a, b, and c, respectively. By plotting $\ln \eta_{rel}/c$ and η_{sp}/c versus concentration, two straight lines with different slopes but similar intercepts were obtained. According to the Huggins and Kraemer's equations, these two intercepts corresponded to the $[\eta]$ derived from each equation. The average value of these two intercepts was calculated as the true $[\eta]$. The obtained $[\eta]$ values were 310.4, 272.6, and 258.8 for CNC-1, CNC-2, and CNC-4, respectively. The as shown $[\eta]$ gradually declined as the aspect ratio of CNCs decreased.

The $[\eta]$ plotted versus f values using the Simha equation are shown in Figure 6d. It is shown that the Simha plot is in a parabola form, in which the $[\eta]$ gradually increased as the f increased. In comparison with the high f region, the increase in $[\eta]$ was much slower at the low aspect ratio region. CNC-1, CNC-2, and CNC-4 had the $[\eta]$ values of 310.4, 272.6, and 258.8, respectively. By substitution of these values into the Simha plot (Figure 6d), the f values were obatined as 69.3, 64.2, and 62.4 for CNC-1, CNC-2, and CNC-4, respectively. The theoretically predicted f values of CNC-1 and CNC-2 are

DOI: 10.1021/acssuschemeng.5b00144
ACS Sustainable Chem. Eng. 2015, 3, 821−832

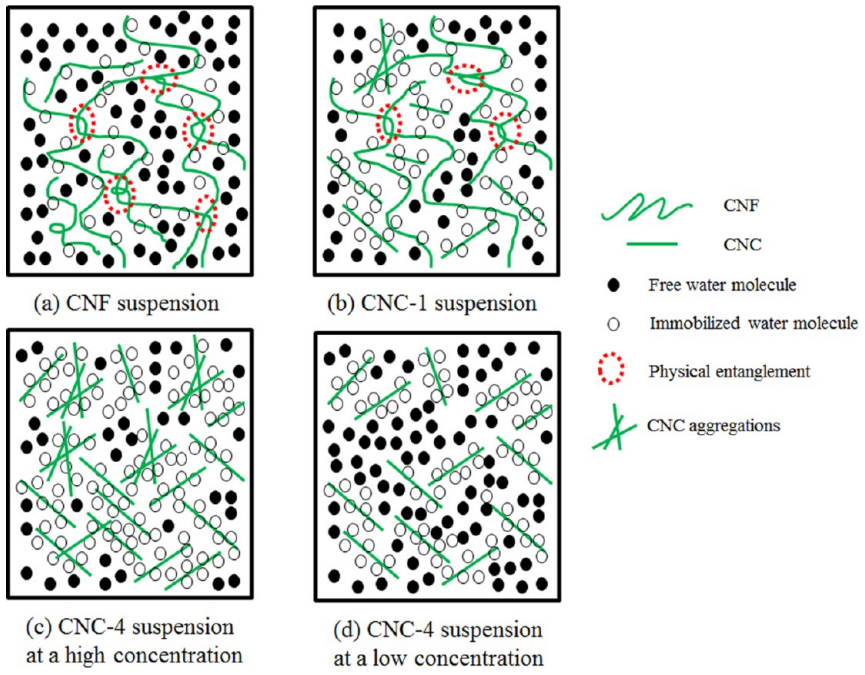

Figure 8. Schematic illustrations of the proposed network of (a) CNF suspension, (b) CNC-1 suspension, (c) CNC-4 suspension at a high concentration, and (d) CNC-4 suspension at a low concentration.

within the range of the f values determined by TEM. However, for CNC-4, the theoretically predicted f value is larger than the value determined by TEM. It should be pointed out that even at the highest shear rate of 1000 s^{-1}, the hydrodynamic interactions between the CNC particles still existed, which led to higher $[\eta]$ values. Another reason might be that CNC-4 carried more sulfate groups than CNC-1 and CNC-2, resulting in more electroviscous effects.[43] After correcting for the hydrodynamic interactions and electroviscous effects, the theoretically predicted values are expected to be well agreed with the TEM results. Nevertheless, the statistical modellling using the Simha equation provided an alternative approach to estimate the f of rod-like particles, showing promising potential in predicting the f of CNCs, which were usually difficult to be clearly observed through the microscopic methods.

Dynamic Rheological Behaviors of CNF and CNC Suspensions. Viscoelastic storage modulus (G') and loss modulus (G'') as a function of angular frequency (ω) of CNF suspensions with different concentrations are shown in Figure 7a. In general, a highly structured solid/gel displayed an elastic rheological behavior, i.e., $G' \approx \omega^0$, $G' \gg G''$, and tan $\delta < 1$. On the contrary, a well dispersed viscous fluid exhibited a viscous rheological behavior, i.e., $G' \approx \omega^2$, $G'' \approx \omega^1$, $G'' \gg G'$, and tan $\delta > 1$.[48,49] For CNF suspensions, both G' and G'' were almost independent of ω, i.e., $G' \approx \omega^0$; and the G' was much higher than G'' in the whole investigated angular frequency ranges, i.e., $G' \gg G''$, indicating the solid-like structure of CNF suspensions. The present CNF suspensions had much higher G' values than the previously reported CNF suspensions mainly due to the formation of a more entangled CNF network because the present CNF had a larger aspect ratio. For example, a 1.5 wt % CNF suspension had a G' of 11090 Pa, which was much higher than 10,000 Pa for 3 wt % of enzymatic hydrolyzed and homogenized softwood CNF suspensions,[12] 5325 Pa for 2.25% homogenized kenaf CNF suspensions,[11] and 5000 Pa for 3.0 wt % homogenized sugar beet CNF suspensions.[15]

Viscoelastic storage modulus (G') and loss modulus (G'') as a function of angular frequency (ω) of CNC-1, CNC-2, and CNC-4 suspensions with concentrations of 1.5, 1.0, 0.5, and 0.25 wt % at 25 °C are shown in Figure 7b, c, and d, respectively. The strong dependence of G' and G'' upon the angular frequency, concentration of CNCs, and aspect ratio of CNCs was observed. For all CNC suspensions, both G' and G'' increased as the angular frequency increased. As the concentration and aspect ratio of the CNCs decreased, the slopes of G' and G'' curves became sharper. CNC suspensions are classified into two types: viscous fluid-like and elastic gel-like. CNC-1 suspensions with concentration of 1.5 and 1.0 wt % exhibited elastic gel-like behavior because they had higher G' than G'' all over the studied angular frequency region (Figure 7b). After the concentration was diluted to 0.5 and 0.25 wt %, they had higher G'' than G', displaying the viscous fluid-like behavior. The phase transition occurred between 0.5 and 1.0 wt %. For CNC-2 suspensions, the elastic gel-like behavior was observed only when the concentration was 1.5 wt %, in which G' and G'' overlapped at the low frequency regions, while G' was higher than G'' at the high frequency regions (Figure 7c). When the concentrations were diluted to 1.0, 0.5, and 0.25 wt %, all suspensions behaved as viscous fluids. The phase transition happened between 1.0 and 1.5 wt %. The CNC-4 suspension displayed viscous-fluid behavior at the whole studied concentration range (Figure 7d). The phase transition took place above 1.5 wt %. Dynamic rheological measurements also revealed that the critical transition concentration was shifted to a higher concentration as the aspect ratio of CNCs decreased, demonstrating strong dependence of the rheological properties and phase transition of CNC suspensions upon the concentration and aspect ratio of CNCs, which was in a good agreement with the steady-flow rheological results.

DOI: 10.1021/acssuschemeng.5b00144
ACS Sustainable Chem. Eng. 2015, 3, 821−832

The dynamic rheological behavior reflected the viscoelastic properties of materials under strain or frequency amplitudes, giving very useful information on predicting the network of materials. In order to better understand the difference in the dynamic rheological behavior of CNF and CNC suspensions, the network of CNF and CNC suspensions were proposed, as illustrated in Figure 8. In a typical CNP suspension, three possible interactions, that is, physical entanglements between CNPs, chemical interactions (e.g., hydrogen bond) between CNPs, and hydrogen bonds between CNP and immobilized water molecules, mainly existed. The differences in the physiochemical characteristics (e.g., aspect ratio, surface properties, flexibility) among CNPs resulted in a distinctive network in the CNP suspensions.

The mechanical disintegrated CNFs showed inactive surface characteristics (e.g., low zeta potential value and fewer hydroxyl groups), larger aspect ratios (>80), and high flexibility, as observed previously. It is believed that the chemical interactions between CNFs and the hydrogen bonds between CNF and water molecule were very weak, whereas the physical entanglements between CNFs were quite strong. Therefore, the network of the CNF suspension mainly contained physical entanglements between CNFs (Figure 8a). The physical entanglements between CNFs could be easily created due to the large aspect ratio and high flexibility of CNFs even at a very low concentration. This is the reason for the observed phenomenon that the CNF suspensions at any concentration level displayed solid-like viscoelastic properties (i.e., $G' \approx \omega^0$, $G' \gg G''$, and $\tan \delta < 1$). By contrast, the sulfuric acid-hydrolyzed CNCs carried negatively charged sulfate groups and a large number of hydroxyl groups on the surface. These highly active groups enabled the CNCs to greatly interact with each other as well as the adjacent water molecules. On the other hand, the needle-like CNCs with relatively low aspect ratios and high crystallinity had worse flexibility than CNFs, leading to the less possibility of formation of a physically entangled network between CNCs. Therefore, in the CNC-4 suspension, the network primarily contained chemical interactions between CNCs as well as hydrogen bonds between CNCs and immobilized water molecules (Figure 8c and d).

The concentration, aspect ratio and surface charges of CNCs had significant influences on the network of CNC suspensions. When the concentration of CNCs was below the critical concentration, the CNC suspension contained more free water molecules, exhibiting viscous liquid-like rheological properties (Figure 8d). In addition, the introduction of sulfate groups on the surface of CNCs generated strong electrostatic repulsion between CNCs, reducing the interparticle interactions, which also contributed to the observed liquid-like rheological behavior. When the concentration of the CNCs was above the critical concentration, the CNC suspension contained more immobilized water molecules and CNC aggregations, displaying elastic gel-like rheological properties (Figure 8c). With an increase in the aspect ratio of CNCs, the possibility of formation of a physically entangled network increased. Therefore, it is expected that in the CNC-1 suspension (Figure 8b), physical entanglements between CNCs with high aspect ratios, chemical interactions between CNCs, and hydrogen bonding between CNCs and immobilized water molecules coexisted, resulting in substantially higher viscoelastic properties than CNC-4 suspension.

CONCLUSIONS

CNCs were extracted from CNFs using sulfuric acid hydrolysis with controlled time, and the changes in the crystalline structure, surface charge, morphology, and rheological behavior were characterized. Acid hydrolysis increased the crystallinity but reduced the length of nanofibers. During acid hydrolysis, sulfate groups were introduced on the surface of CNCs, which was also enhanced with an increase in hydrolysis time. During the freeze-drying process, CNCs self-assembled into lamellar foam composed of thin membranes, whereas a similar self-assembling behavior did not occur for CNFs. After freeze-drying, the rigid entangled network of nanofibers was well kept. The CNF suspensions exhibited rigid solid-like viscoelastic properties even at a very low concentration owing to the formation of a highly entangled network. As the concentration of CNFs increased, the viscosity, storage modulus, and loss modulus gradually increased. Acid hydrolysis caused a significant loss of rheological properties due to a profound reduction in the dimension and entangled network. The rheological behavior of the CNC suspensions showed a significant dependence on the concentration and aspect ratio of CNCs. With a change in the amount of free/immobilized water molecules, the CNC suspensions formed elastic gel-like materials at high concentrations but viscous liquid-like materials at low concentrations. Longer acid hydrolysis time produced CNCs with lower aspect ratios, leading to higher critical transition concentration for the formation of the anisotropic phase. The intrinsic viscosity values of CNCs, determined using Huggins and Kraemer's equations, decreased as the aspect ratio of CNCs decreased. With the aid of the Simha's equation for CNCs, the theoretically predicted aspect ratio values well agreed with the TEM results.

This work addresses the changes in the crystallinity, surface charge, morphology, and rheological properties of CNFs upon hydrolysis, the relationship between aspect ratio and rheological properties of CNC suspensions, and the relationship between concentration and rheological properties of CNP suspensions. A desired rheological property can be tailored by adjusting CNP processing conditions (e.g., hydrolysis time) and concentration, providing practical guidance and scientific information on the preparation and development of novel rheology-dependent CNP based-materials, such as food, paints, and drilling fluids.

AUTHOR INFORMATION

Corresponding Authors

*E-mail: qwu@agcenter.lsu.edu. Phone: 225-578-8369. Fax: 225-578-4251.

*E-mail: wuyiqiang@csuft.edu.cn. Phone: 731-85623301. Fax: 731-85623301.

Author Contributions

The manuscript was written through contributions of all authors. All authors have given approval to the final version of the manuscript.

Notes

The authors declare no competing financial interest.

ACKNOWLEDGMENTS

This collaborative study was carried out with support from the Louisiana Board of Regents [LEQSF-EPS (2014)-OPT-IN-37, LEQSF(2013-14)-ENH-TR-02], Central South University of Forestry and Technology, Changsha, China, and Collaborative

DOI: 10.1021/acssuschemeng.5b00144
ACS Sustainable Chem. Eng. 2015, 3, 821−832

Innovation Center of Biomass Energy of Henan Province, Henan Agricultural University, Zhengzhou, China.

REFERENCES

(1) Xu, X.; Liu, F.; Jiang, L.; Zhu, J. Y.; Haagenson, D.; Wiesenborn, D. P. Cellulose Nanocrystals vs. Cellulose Nanofibrils: A Comparative Study on Their Microstructures and Effects as Polymer Reinforcing Agents. *ACS Appl. Mater. Interfaces* **2013**, *5*, 2999−3009.

(2) Salam, A.; Lucia, L. A.; Jameel, H. A Novel Cellulose Nanocrystals-Based Approach To Improve the Mechanical Properties of Recycled Paper. *ACS Sustainable Chem. Eng.* **2013**, *1*, 1584−1592.

(3) Yu, H.-Y.; Qin, Z.-Y.; Yan, C.-F.; Yao, J.-M. Green Nanocomposites Based on Functionalized Cellulose Nanocrystals: A Study on the Relationship between Interfacial Interaction and Property Enhancement. *ACS Sustainable Chem. Eng.* **2014**, *2*, 875−886.

(4) Bayati, F.; Boluk, Y.; Choi, P. Diffusion Behavior of Water at Infinite Dilution in Hydroxypropyl Xylan Films with Sorbitol and Cellulose Nanocrystals. *ACS Sustainable Chem. Eng.* **2014**, *2*, 1305−1311.

(5) Zhou, C.; Shi, Q.; Guo, W.; Terrell, L.; Qureshi, A. T.; Hayes, D. J.; Wu, Q. Electrospun Bio-Nanocomposite Scaffolds for Bone Tissue Engineering by Cellulose Nanocrystals Reinforcing Maleic Anhydride Grafted PLA. *ACS Appl. Mater. Interfaces* **2013**, *5*, 3847−3854.

(6) Zhou, C.; Wu, Q.; Yue, Y.; Zhang, Q. Application of Rod-Shaped Cellulose Nanocrystals in Polyacrylamide Hydrogels. *J. Colloid Interface Sci.* **2011**, *353*, 116−123.

(7) Yang, X.; Cranston, E. D. Chemically Cross-Linked Cellulose Nanocrystal Aerogels with Shape Recovery and Superabsorbent Properties. *Chem. Mater.* **2014**, *26*, 6016−6025.

(8) Chen, L.; Berry, R. M.; Tam, K. C. Synthesis of β-Cyclodextrin-Modified Cellulose Nanocrystals (CNCs)@Fe_3O_4@SiO_2 Superparamagnetic Nanorods. *ACS Sustainable Chem. Eng.* **2014**, *2*, 951−958.

(9) Wang, H.; Zhu, E.; Yang, J.; Zhou, P.; Sun, D.; Tang, W. Bacterial Cellulose Nanofiber-Supported Polyaniline Nanocomposites with Flake-Shaped Morphology as Supercapacitor Electrodes. *J. Phys. Chem. C* **2012**, *116*, 13013−13019.

(10) Pan, J.; Hamad, W.; Straus, S. K. Parameters Affecting the Chiral Nematic Phase of Nanocrystalline Cellulose Films. *Macromolecules* **2010**, *43*, 3851−3858.

(11) Rezayati Charani, P.; Dehghani-Firouzabadi, M.; Afra, E.; Shakeri, A. Rheological Characterization of High Concentrated MFC Gel from Kenaf Unbleached Pulp. *Cellulose* **2013**, *20*, 727−740.

(12) Pääkkö, M.; Ankerfors, M.; Kosonen, H.; Nykänen, A.; Ahola, S.; Österberg, M.; Ruokolainen, J.; Laine, J.; Larsson, P. T.; Ikkala, O.; Lindstrom, T. Enzymatic Hydrolysis Combined with Mechanical Shearing and High-Pressure Homogenization for Nanoscale Cellulose Fibrils and Strong Gels. *Biomacromolecules* **2007**, *8*, 1934−1941.

(13) Benhamou, K.; Dufresne, A.; Magnin, A.; Mortha, G.; Kaddami, H. Control of Size and Viscoelastic Properties of Nanofibrillated Cellulose from Palm Tree by Varying the TEMPO-Mediated Oxidation Time. *Carbohydr. Polym.* **2014**, *99*, 74−83.

(14) Damani, R.; Powell, R. L.; Hagen, N. Viscoelastic Characterization of Medium Consistency Pulp Suspensions. *Can. J. Chem. Eng.* **1993**, *71*, 676−684.

(15) Agoda-Tandjawa, G.; Durand, S.; Berot, S.; Blassel, C.; Gaillard, C.; Garnier, C.; Doublier, J.-L. Rheological Characterization of Microfibrillated Cellulose Suspensions after Freezing. *Carbohydr. Polym.* **2010**, *80*, 677−686.

(16) Wu, Q.; Meng, Y.; Wang, S.; Li, Y.; Fu, S.; Ma, L.; Harper, D. Rheological Behavior of Cellulose Nanocrystal Suspension: Influence of Concentration and Aspect Ratio. *J. Appl. Polym. Sci.* **2014**, *131*, n/a−n/a.

(17) Shafiei-Sabet, S.; Hamad, W. Y.; Hatzikiriakos, S. G. Rheology of Nanocrystalline Cellulose Aqueous Suspensions. *Langmuir* **2012**, *28*, 17124−17133.

(18) Shafiei-Sabet, S.; Hamad, W. Y.; Hatzikiriakos, S. G. Influence of Degree of Sulfation on the Rheology of Cellulose Nanocrystal Suspensions. *Rheol. Acta* **2013**, *52*, 741−751.

(19) Shafiei-Sabet, S.; Hamad, W. Y.; Hatzikiriakos, S. G. Ionic Strength Effects on the Microstructure and Shear Rheology of Cellulose Nanocrystal Suspensions. *Cellulose* **2014**, *21*, 3347−3359.

(20) Ureña-Benavides, E. E.; Ao, G.; Davis, V. A.; Kitchens, C. L. Rheology and Phase Behavior of Lyotropic Cellulose Nanocrystal Suspensions. *Macromolecules* **2011**, *44*, 8990−8998.

(21) Dong, X. M.; Kimura, T.; Revol, J.-F.; Gray, D. G. Effects of Ionic Strength on the Isotropic−Chiral Nematic Phase Transition of Suspensions of Cellulose Crystallites. *Langmuir* **1996**, *12*, 2076−2082.

(22) Beck-Candanedo, S.; Roman, M.; Gray, D. G. Effect of Reaction Conditions on the Properties and Behavior of Wood Cellulose Nanocrystal Suspensions. *Biomacromolecules* **2005**, *6*, 1048−1054.

(23) Bercea, M.; Navard, P. Shear Dynamics of Aqueous Suspensions of Cellulose Whiskers. *Macromolecules* **2000**, *33*, 6011−6016.

(24) Liu, H.; Liu, D.; Yao, F.; Wu, Q. Fabrication and Properties of Transparent Polymethylmethacrylate/Cellulose Nanocrystals Composites. *Bioresour. Technol.* **2010**, *101*, 5685−5692.

(25) Han, J.; Zhou, C.; Wu, Y.; Liu, F.; Wu, Q. Self-Assembling Behavior of Cellulose Nanoparticles during Freeze-Drying: Effect of Suspension Concentration, Particle Size, Crystal Structure, and Surface Charge. *Biomacromolecules* **2013**, *14*, 1529−1540.

(26) Segal, L.; Creely, J. J.; Martin, A. E.; Conrad, C. M. An Empirical Method for Estimating the Degree of Crystallinity of Native Cellulose Using the X-ray Diffractometer. *Text. Res. J.* **1959**, *29*, 786−794.

(27) Hamad, W. Y.; Hu, T. Q. Structure−process−yield Interrelations in Nanocrystalline Cellulose Extraction. *Can. J. Chem. Eng.* **2010**, *88*, 392−402.

(28) French, A. Idealized Powder Diffraction Patterns for Cellulose Polymorphs. *Cellulose* **2014**, *21*, 885−896.

(29) Yu, H.; Yan, C.; Lei, X.; Qin, Z.; Yao, J. Novel Approach To Extract Thermally Stable Cellulose Nanospheres with High Yield. *Mater. Lett.* **2014**, *131*, 12−15.

(30) Zuluaga, R.; Putaux, J. L.; Cruz, J.; Vélez, J.; Mondragon, I.; Gañán, P. Cellulose microfibrils from Banana Rachis: Effect of Alkaline Treatments on Structural and Morphological Features. *Carbohydr. Polym.* **2009**, *76*, 51−59.

(31) Rosa, M. F.; Medeiros, E. S.; Malmonge, J. A.; Gregorski, K. S.; Wood, D. F.; Mattoso, L. H. C.; Glenn, G.; Orts, W. J.; Imam, S. H. Cellulose Nanowhiskers from Coconut Husk Fibers: Effect of Preparation Conditions on Their Thermal and Morphological Behavior. *Carbohydr. Polym.* **2010**, *81*, 83−92.

(32) Ribitsch, V.; Stana-Kleinschek, K.; Jeler, S. The Influence of Classical and Enzymatic Treatment on the Surface Charge of Cellulose Fibres. *Colloid Polym. Sci.* **1996**, *274*, 388−394.

(33) Iwamoto, S.; Lee, S.; Endo, T. Relationship between Aspect Ratio and Suspension Viscosity of Wood Cellulose Nanofibers. *Polym. J.* **2013**, *46*, 73−76.

(34) Kalia, S.; Boufi, S.; Celli, A.; Kango, S. Nanofibrillated Cellulose: Surface Modification and Potential Applications. *Colloid Polym. Sci.* **2014**, *292*, 5−31.

(35) Everett, D. H. *Basic Principles of Colloid Science*; Royal Society of Chemistry: London, 1988.

(36) Lin, N.; Dufresne, A. Surface Chemistry, Morphological Analysis and Properties of Cellulose Nanocrystals with Gradiented Sulfation Degrees. *Nanoscale* **2014**, *6*, 5384−5393.

(37) Pei, A.; Malho, J.-M.; Ruokolainen, J.; Zhou, Q.; Berglund, L. a. Strong Nanocomposite Reinforcement Effects in Polyurethane Elastomer with Low Volume Fraction of Cellulose Nanocrystals. *Macromolecules* **2011**, *44*, 4422−4427.

(38) Kargarzadeh, H.; Ahmad, I.; Abdullah, I.; Dufresne, A.; Zainudin, S. Y.; Sheltami, R. M. Effects of Hydrolysis Conditions on the Morphology, Crystallinity, And Thermal Stability of Cellulose Nanocrystals Extracted from Kenaf Bast Fibers. *Cellulose* **2012**, *19*, 855−866.

(39) Jiang, F.; Hsieh, Y.-L. Chemically and Mechanically Isolated Nanocellulose and Their Self-Assembled Structures. *Carbohydr. Polym.* **2013**, *95*, 32−40.

DOI: 10.1021/acssuschemeng.5b00144
ACS Sustainable Chem. Eng. 2015, 3, 821−832

(40) Lu, P.; Hsieh, Y.-L. Preparation and Characterization of Cellulose Nanocrystals from Rice Straw. *Carbohydr. Polym.* **2012**, *87*, 564−573.
(41) Iotti, M.; Weiby, Ø.; Moe, S.; Lenes, M. Rheological Studies of Microfibrillar Cellulose Water Dispersions. *J. Polym. Environ.* **2011**, *19*, 137−145.
(42) Araki, J.; Wada, M.; Kuga, S.; Okano, T. Flow Properties of Microcrystalline Cellulose Suspension Prepared by Acid Treatment of Native Cellulose. *Colloids Surf., A* **1998**, *142*, 75−82.
(43) Boluk, Y.; Lahiji, R.; Zhao, L.; McDermott, M. T. Suspension viscosities and shape parameter of cellulose nanocrystals (CNC). *Colloids Surf., A* **2011**, *377*, 297−303.
(44) Simha, R. The Influence of Brownian Movement on the Viscosity of Solutions. *J. Phys. Chem.* **1940**, *44*, 25−34.
(45) Osman, M. A.; Atallah, A.; Schweizer, T.; Öttinger, H. C. Particle−Particle and Particle−Matrix Interactions in Calcite Filled High-Density Polyethylene—Steady Shear. *J. Rheol.* **2004**, *48*, 1167−1184.
(46) Huggins, M. L. The Viscosity of Dilute Solutions of Long-Chain Molecules. IV. Dependence on Concentration. *J. Am. Chem. Soc.* **1942**, *64*, 2716−2718.
(47) Kraemer, E. O. Molecular Weights of Celluloses and Cellulose Derivates. *Ind. Eng. Chem.* **1938**, *30*, 1200−1203.
(48) Ross-Murphy, S. B. Rheological Characterization of Polymer Gels and Networks. *Polym. Gels Networks* **1994**, *2*, 229−237.
(49) Kavanagh, G. M.; Ross-Murphy, S. B. Rheological Characterisation of Polymer Gels. *Prog. Polym. Sci.* **1998**, *23*, 533−562.

DOI: 10.1021/acssuschemeng.5b00144
ACS Sustainable Chem. Eng. 2015, 3, 821−832